Wind-Driven Inertial Currents in the Magdalen Shallows, Gulf of St. Lawrence

B. L. BLACKFORD[1]

Physics Department, Dalhousie University, Halifax, N.S., Canada B3H 3J5

(Manuscript received 16 December 1976, in final form 14 March 1978)

ABSTRACT

Power spectrum analyses of the residual current components from the Magdalen Shallows (autumn 1970) gave a prominent peak at the inertial frequency. Bandpass filtering showed that the inertial oscillations occurred in bursts of 2–3 days duration and with irregular intervals between bursts. The transient nature of the above behavior was consistent with the pulselike nature of the wind stress and a convincing linear correlation was found between the magnitude of the wind stress and the rms residual current. Using a simple slab model with a linear drag law, it was found that the transient response to a typical wind stress pulse was also pulselike, with a relatively small phase lag. The magnitude of the response was found to be a sensitive function of the duration of the wind stress pulse. Comparison of the theory with the experimental results indicates that the simple slab model is a good approximation. The results suggest that, on average, about 50% of the residual current speed was due to the local wind.

1. Introduction

An analysis is presented of current meter data collected in the Magdalen Shallows, Gulf of St. Lawrence, during the autumn of 1970 (BIO Cruise No. 70-036). The analysis is mainly concerned with inertial type events having periods of less than a day or two. (The period of pure inertial oscillations ranges from 16.0 to 16.5 h in the region of interest.) The records were approximately 22 days in length and derive from 10 current meter stations (19 current meters in all) situated at various locations in the Magdalen Shallows (Fig. 1).

Power spectrum analyses of the residual current components (u and v) showed a prominent peak at the inertial frequency, particularly for the current meters located above the pycnocline depth of 40 m. (In this paper, *residual current* means total current minus the tidal constituents.) Bandpass filtering at the inertial frequency of the residual current records showed that the inertial oscillations occurred in bursts of two or three days duration and with irregular spacing between bursts. Attempts to correlate the bursts of inertial oscillations with wind data from shore-based weather stations were not very successful. A convincing linear correlation, however, was found between the square of the wind speed and the root-mean-square (rms) values of the residual current speed, i.e., $[(u^2 + v^2)_{av}]^{1/2}$. The average (av) refers to a spatial average taken over several current meter stations, excluding the three stations (No. 78, 79 and 80 in Fig. 1) located close to the Gaspé Coast.

The theoretical behavior of the system was investigated using a simple slab model with wind forcing and a linear drag law, similar to that used by Pollard and Millard (1970). The transient response of the model to a typical wind stress pulse was found to be pulselike with a relatively small phase lag. The magnitude of the response was found to depend quite sensitively on the duration of the wind stress pulse. The maximum response was found when the pulse duration was approximately equal to the inertial period. This result is somewhat surprising as it seems at first glance to disagree with a conclusion of Pollard and Millard (1970). Comparison of the theory with the experimental results allows one to obtain values for the surface wind drag coefficient and the bottom drag coefficient, respectively. The values thereby obtained are in reasonable agreement with the currently accepted values for these coefficients, which indicates that the simple slab model is a good approximation.

The results suggest that, on average, about 50% of the residual current speed in the Magdalen Shallows was due to the local wind. During periods of high wind (>15 m s^{-1}) the wind-driven current probably dominates. However, this was not the case for Stations 78, 79 and 80, which were dominated by the comparatively strong Gaspé Current. [Farquharson (1966) gives a description of the Gaspé Current.] The residual currents at the latter three stations were poorly correlated with the local

[1] This work was done while on sabbatical leave (1975–76) at Atlantic Oceanographic Laboratory, Bedford Institute of Oceanography, Dartmouth, N.S., Canada.

0022-3670/78/0653-0664$06.00

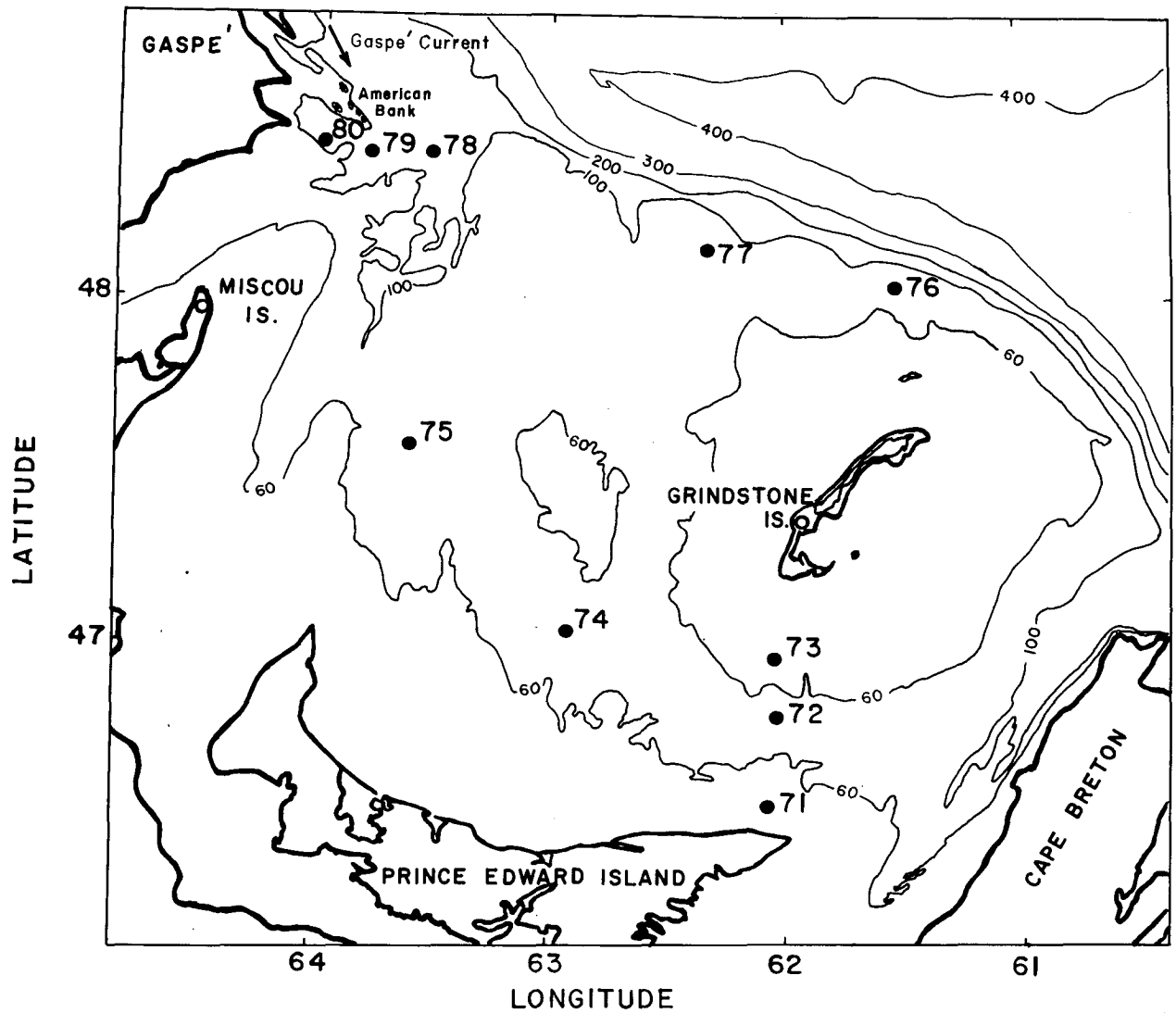

FIG. 1. Map of the Magdalen Shallows region showing the locations of current meters and weather stations. Depth contours are in meters.

wind. The results from these three stations will be discussed elsewhere.

2. Current meter data

a. Tidal analysis

Film recording Braincon Type 316 and 381 current meters were used with a recording interval of 20 min. The 22-day records were analysed with a standard 15-day tidal analysis program to remove the coherent signal at six frequencies corresponding to the K_1, O_1, M_2, S_2, M_4 and MS_4 tidal constituents. The amplitude of the M_2 constituent varied from a minimum of 6 cm s^{-1} at Station 73-49 m to a maximum of 17 cm s^{-1} at Station 77-26 m. The M_4 and MS_4 constituents were typically an order of magnitude less than M_2.

After removing the tidal constituents the residuals were low-pass filtered with a 2 h cutoff and files of the residual u and v velocity components were created at 1 h intervals, where u is positive east and v is positive north. The filter used was a $(\sin x)/x$ type in the time domain. Table 1 shows the mean values of the residual current components averaged over the entire record. The rms speeds and the rms deviations are also given in Table 1. The mean residual currents are reasonably consistent with the geostrophic flow patterns depicted by El-Sahb (1975).

The pycnocline depth during the period of the measurements was about 40 m (Taylor, 1975), and it can be seen from Table 1 that the residual currents are much stronger above the pycnocline than below it. The tidal currents were much more

barotropic than the residuals. It should be noted that the majority of the current meters below the pycnocline were within a few meters of the bottom.

b. Power spectra

The hourly residual current files from each current meter record were analysed by the Fast Fourier Transform Spectral Analysis programme of Dobson *et al.* (1974). The data were divided into four blocks of 128 samples (hours) each, which yielded Fourier coefficients at 13 frequencies ranging from 0.007 to 0.4 cph. The Fourier coefficients were hanned by the spectral analysis program.

Fig. 2 shows a plot of the power spectra of the residual u and v velocity components at Station 74-19 m. The logarithm of frequency x spectrum is plotted versus the logarithm of the frequency. The most interesting feature is the dominant peak at the frequency closest to the inertial frequency. This was a common feature of the data from above the pycnocline, as can be seen from Fig. 3a which gives the average combined spectra of u and v from eight current meters. Fig. 3a shows that the mean amplitude of the currents at the inertial frequency was about 10 cm s^{-1}, above the pycnocline. This is the same order of magnitude as the amplitude of the largest tidal constituent, M_2, and also of the mean residual velocity components $\bar{u}$ and $\bar{v}$.

The average combined spectrum of u and v from six current meters located below the pycnocline is shown in Fig. 3b. The spectrum is typically an order of magnitude weaker at all frequencies than that from above the pycnocline and the shape is also somewhat different. The peak at the inertial frequency is greatly reduced in comparison with the remainder of the spectrum and the entire spectrum is weighted more toward the high-frequency end. The reason for the latter behavior is not known.

c. Coherence and phase

The spectral analysis program of Dobson *et al.* also calculates coherence and phase differences between the various data channels analysed. These are useful when considering inertial motion. Fig. 4 shows a plot of coherence and phase difference between u and v for Station 74-19 m. The vertical error bar on the phase values indicates the scatter of the measured phase among the four blocks into which the data were divided for analysis purposes. The dashed line gives the 95% confidence level for the coherences. It can be seen that the coherence at the inertial frequency is well above the 95% confidence level. Furthermore, the phase difference at this frequency is near $-90°$ and has a relatively small error. A phase difference of $-90°$ corresponds to v leading u by 90°, which is to be expected for the clockwise water movements associated with pure inertial motion.

TABLE 1. Various mean values of the residual velocity components for each current meter.

Station	Depth (m)	Mean velocity (cm s^{-1}) $\bar{u}$	Mean velocity (cm s^{-1}) $\bar{v}$	$\sqrt{\text{Variance}}$ (cm s^{-1}) u	$\sqrt{\text{Variance}}$ (cm s^{-1}) v	Mean speed $[(u^2 + v^2)]^{1/2}$ (cm s^{-1})
71	43	4.9	0.3	7.2	6.9	11.1
72	17	18	−2.2	11	9.5	22.7
73	49	0.6	−0.5	2.5	2.3	3.5
74	19	3.8	−8.9	8.4	10.0	16.2
	29	5.5	−9.3	9.7	10.6	18.0
	54	2.3	−2.4	4.9	5.0	7.8
75	16	0.9	−4.4	7.5	7.8	11.8
	25	4.3	−9.4	12.3	11.9	20.0
	69	−0.2	−1.0	4.8	4.8	6.9
76	15	5.6	−3.1	10.2	10.2	15.8
	61	4.7	1.2	5.2	4.3	8.3
77	26	−5.2	−1.5	14.1	13.3	20.0
78	21	3.5	−7.2	13.6	12.1	19.9
	81	3.6	1.8	7.3	7.6	11.3
79	15	−13	−30	32.1	15.7	48.3
	125	0	−1.7	10.3	6.1	12.1
80	15	−9.2	−2.9	16.8	14.4	24.1
	75	5.2	−0.2	11.0	11.4	16.7
	104	0.2	−1.2	3.3	2.7	4.4

Fig. 5 shows the average coherence and average phase for eight current meters located above the pycnocline. In this figure the error bar on the phase values gives the rms deviation, divided by $\sqrt{8}$, for the eight current meters involved. The average coherence (0.81 ± 0.1 rms deviation) at the inertial frequency is considerably above the 95% level and the average phase is $-93°$ ± 10° rms deviation. At nearly all other frequencies the coherences are less than the 95% level and the scatter in the phases is much greater. The average coherence and average phase for six current meters located below the pycnocline were also calculated. The coherence at the inertial frequency was slightly above the 95% level but the average phase was $-50°$ ± 80° rms deviation.

Summarizing the results of the spectral analysis, it can be said that inertial motion is a statistically significant aspect of the residual (non-tidal) currents above the pycnocline in the Magdalen Shallows, at least for the period of these observations from mid-October to mid-November 1970.

d. Bandpass filtering

Having shown, via spectral analysis, the existence of inertial motion in the current meter records it is

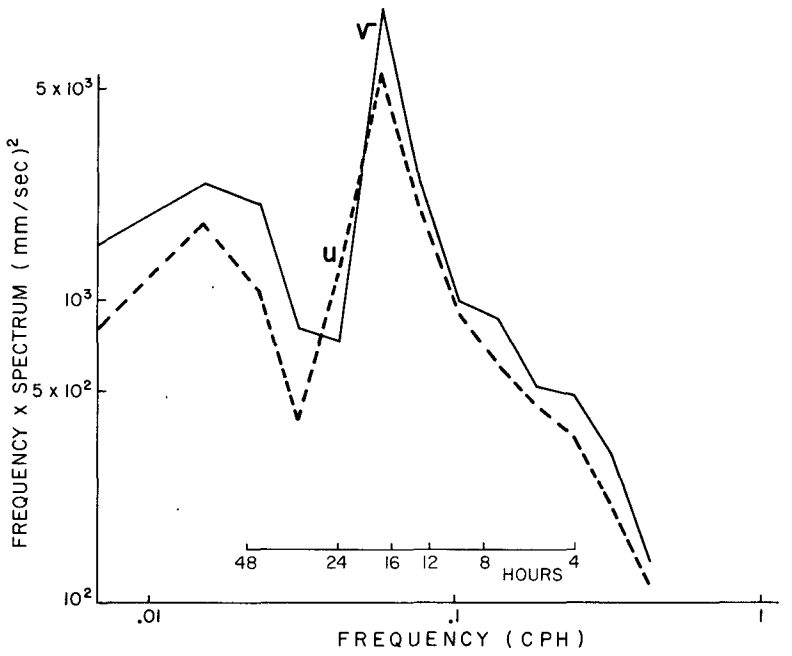

FIG. 2. Power spectra of the residual u and v velocity components at Station 74-19 m.

useful to look at its time dependence. That is, how does the amplitude of the inertial motion vary with time throughout the record? One way of looking at the time dependence is to filter the residual current data files with a bandpass filter centered at the inertial frequency. This was done for the residual current files from above the pycnocline using a Cartwright type of bandpass filter. The particular filter used had a center frequency of 0.0650 cph (15.5 h period) and a maximum response factor of

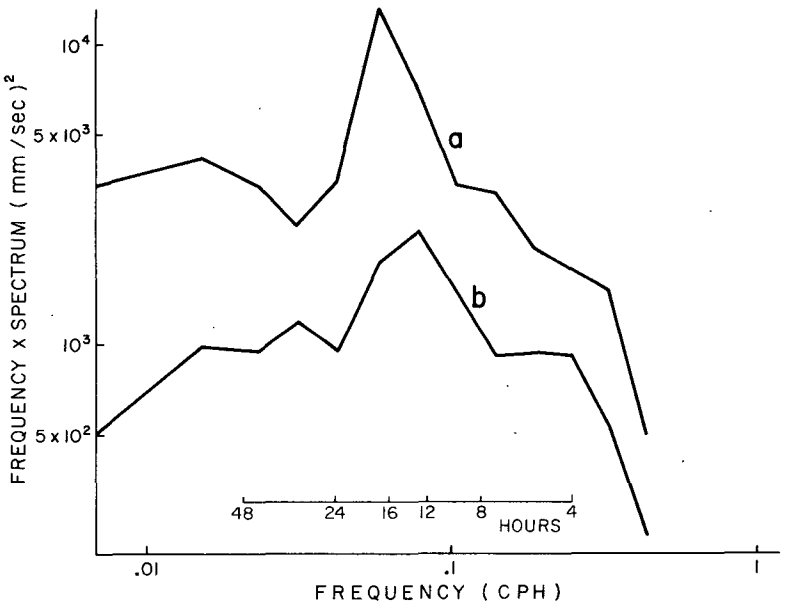

FIG. 3. Average combined spectra of u and v from (a) above the pycnocline and (b) below the pycnocline. Curve (a) is an average of current meters at Stations 72-17 m, 74-19, 29 m, 75-16, 25 m, 77-26 m and 78-21 m. Curve (b) is an average of Stations 71-43 m, 73-49 m, 74-54 m, 75-69 m, 76-61 m and 78-81 m. Note that Stations 79 and 80 are excluded.

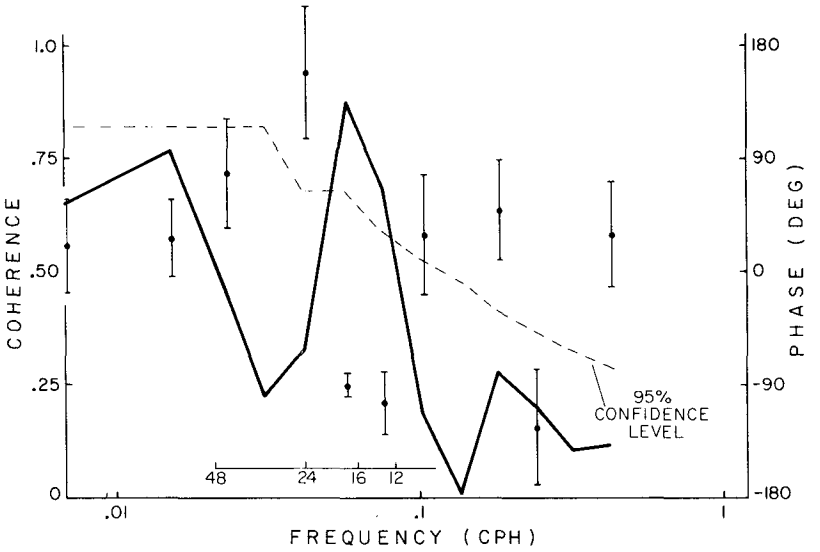

FIG. 4. Coherence and phase difference between the residual u and v velocity components at Station 74-19 m.

0.7. The response was down by a factor of 2 at frequencies of 0.0566 cph (17.7 h period) and 0.0732 cph (13.7 h period), giving a half amplitude bandwidth of 0.0166 cph.

Fig. 6 shows the bandpassed u and v velocity components from Station 75-16 m as a function of time. Considerable time dependence is evident, with a pronounced minimum occurring near day 306. Examination of the rate of decay gives an e-folding time of about two days, or three inertial periods. The amplitude of the inertial motion is expected to be a more convenient way to look at the time dependence and the square of the amplitude $(u^2 + v^2)$ is plotted in Fig. 7 using the same data as in Fig. 6. Examination of Fig. 7 indicates that the inertial motion occurs in bursts of about three days duration with irregular spacing between bursts. The high-frequency (actually twice the inertial frequency) signal superimposed on the inertial amplitude in Fig. 7 is a result of the squaring process. It arises because the amplitudes of the u and v components at the inertial frequency are not identical, as can be seen in Fig. 6. The effect appears to be more pronounced during the buildup of the inertial peaks. The phase relation between u and v can be seen from Fig. 6. It is easy to see that v leads u by about 90°, although this phase relation is not maintained during periods of low amplitude.

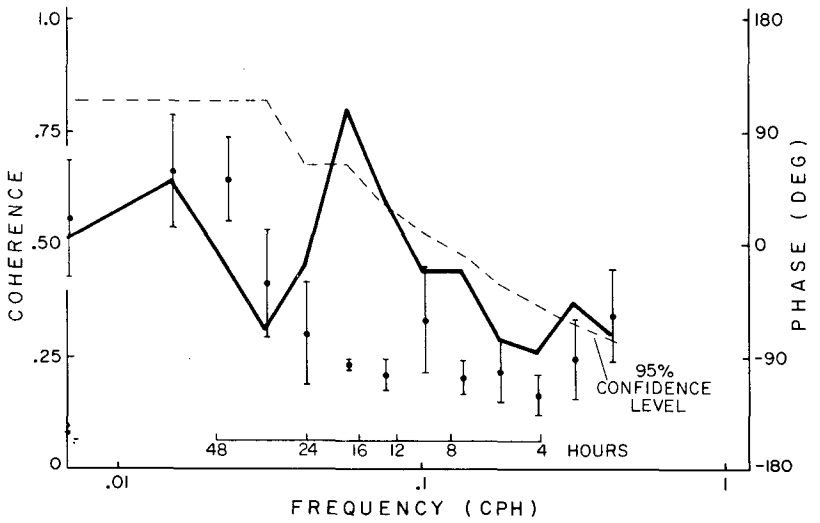

FIG. 5. Average coherence and average phase for selected current meters located above the pycnocline.

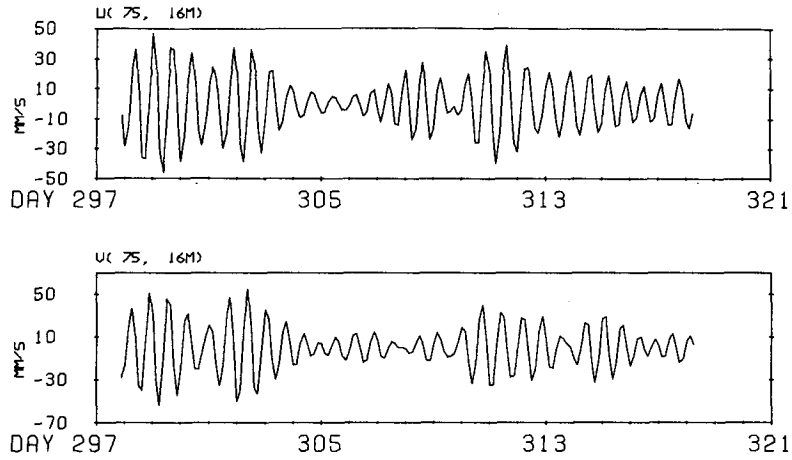

FIG. 6. Bandpassed (at the inertial frequency) u and v velocity components at Station 75-16 m.

It could be said that the decay rate of the bandpassed records may not accurately represent the decay rate of the inertial oscillations. This is because the filter itself can introduce an artificial decay, as shown by Kundu (1976), for example. To check that this was not happening here we applied several bandpass filters of greater bandwidths (up to 0.05 cph) to the data of Station 75-16 m. The results obtained showed slightly shorter rise times at the leading edges of the pulses but gave essentially the same decay rates as those shown in Figs. 6 and 7. In this regard, it should be noted that the decay times are considerably longer than the rise times for a typical pulse (e.g., Fig. 7). If the decay rates were due to the filter one would expect a symmetrical rise and fall of the pulse, Kundu (1976). A complex demodulation program was also applied to the data and this gave results in agreement with the bandpass filtering, i.e., asymmetrical amplitude pulses which rise faster than they decay. For these reasons, we are confident that the decay rates observed here are not filter limited.

The bandpass filter was applied to all of the residual current files from above the pycnocline and each gave results similar to those shown in Figs. 6 and 7. However, the bursts of inertial motion did not occur simultaneously at all current meter stations and the actual measured decay times varied by as much as a factor of two (see Section 4) among the various pulses.

We remind the reader at this point that the original data was filtered by a tidal analysis program prior to the bandpass filtering at the inertial frequency. The effect of this is assumed to be negligible, although it is somewhat unknown.

e. *Spatial coherence*

The coherences discussed thus far have been between the u and v velocity components at the same current meter location. It is also of interest to look at coherences between velocity components at different positions.

Fig. 8 shows the coherence and phase difference between the v components of velocity at Station 74-19 m and 29 m. Generally speaking, the coherence is above the 95% level up to frequencies corresponding to periods of about 5 h, with a particularly high value at the inertial frequency. The phase differences are close to zero, where positive phase corresponds to the v component at 19 m depth leading the v component at 29 m depth. The slightly negative phase at the inertial frequency suggests downward energy propagation, which is to be expected.

In Fig. 8, which gives high coherence, the two

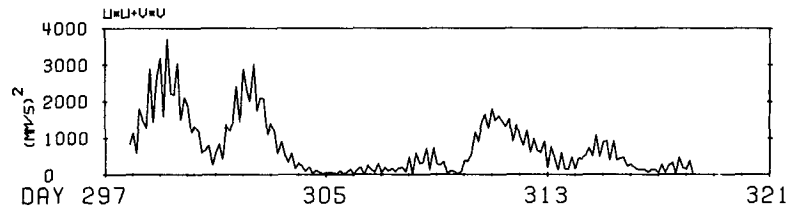

FIG. 7. Sum of the squares of the bandpassed u and v velocity components at Station 75-16 m.

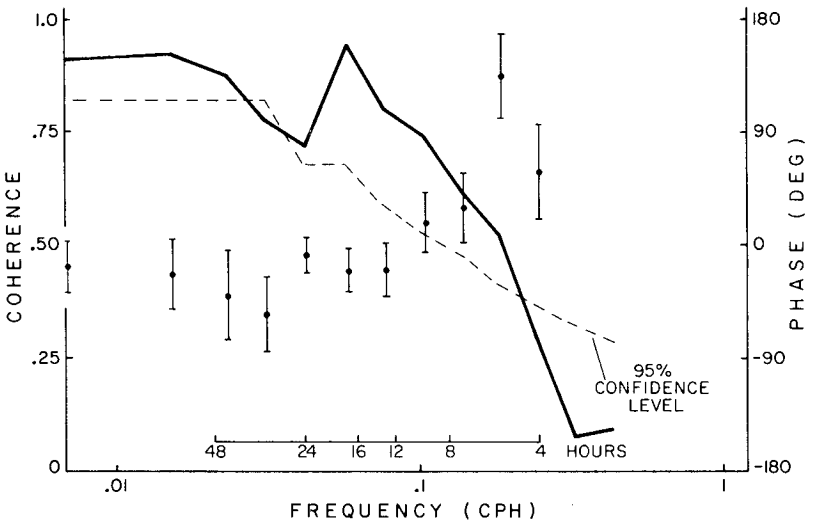

FIG. 8. Coherence and phase difference between the v velocity components at Station 74-19 m and 29 m.

current meters involved were both located above the pycnocline. On the other hand, for two current meters situated one above and one below the pycnocline, such as Station 75-25 m and 69 m, significant coherence was *not* obtained at any frequency. The coherence between currents at different mooring locations was also generally very poor at all frequencies.

3. Correlation of wind and current data

For making comparisons between wind and current data it would be ideal to have wind data from the same location as the current meter station. Unfortunately, this was not the case here and therefore data from shorebased weather stations was used to obtain an idea of the wind field over the Magdalen Shallows. Fig. 9 shows a time series plot of the square of the wind speed from the weather station at Grindstone Island, which is situated in the Magdalen Islands complex on the eastern portion of the Magdalen Shallows (Fig. 1). The original wind record was in the form of hourly values of rate and direction. Examination of Fig. 9 shows that the magnitude of the wind stress (here it is being assumed that wind stress is proportional to the square of the wind speed) is characterized by pulses of 1–2 days duration separated by periods of relative calm. The separation between the pulses varies from less than a day to about four days.

An attempt was made to correlate the bursts of inertial oscillations, of the type shown in Fig. 7, with the wind stress data of Fig. 9. Although some of the inertial peaks were obviously associated with particular wind events, the correlation on the whole was very poor. For example, the inertial peak centered at day 311 in Fig. 7 appears to be caused by the wind stress pulse occurring on day 310 in Fig. 9. In contrast to this, a similar wind stress peak on day 308 produced only a small inertial oscillation. The situation was further complicated by the variability of the inertial peaks from station to station.

The above behavior is not inconsistent with the observations of Pollard and Millard (1970) who point out that the generation of pure inertial oscillations depends not only on the local wind stress but also on the initial value of the local current velocity. The duration in time of the wind stress pulse is also very important for determining the amplitude of inertial motion which is generated, as we show in the theoretical discussion of Section 4.

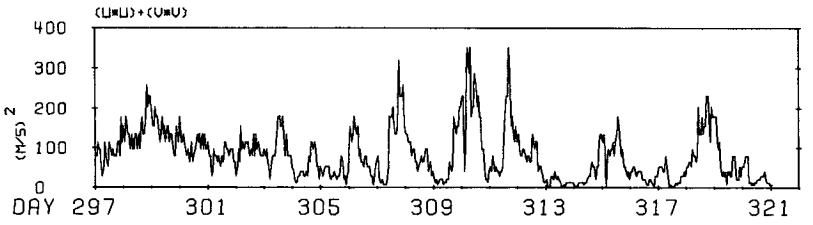

FIG. 9. Square of the wind speed at Grindstone Island weather station.

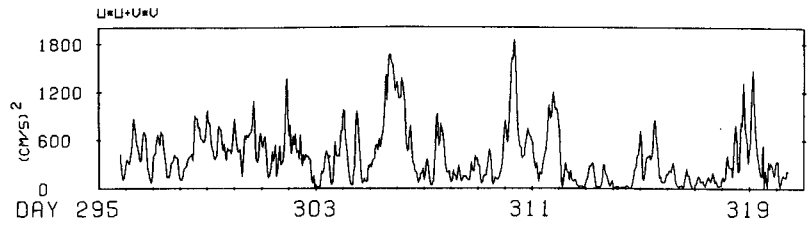

FIG. 10. Sum of the squares $(u^2 + v^2)$ of the residual velocity components at Station 75-25 m.

More encouraging results were found when plots of the residual current speed (or square of the speed) versus time were created. Fig. 10 shows $(u^2 + v^2)$ plotted versus time for Station 75-25 m. Comparison with Fig. 9 shows that the peaks in $(u^2 + v^2)$ are in good correspondence with the peaks in the square of the wind speed. The correlation is more readily apparent in Fig. 11 where the rms residual current is plotted together with the mean-square wind speed. The rms residual current was obtained by adding $(u^2 + v^2)$ from eight current meters located above the pycnocline, taking their mean and then the square root. (Note that Stations 78, 79 and 80 were not included in the average.) The mean-square wind speed is the average of wind speed squared for Grindstone and Miscou Islands weather stations. Miscou Island is located on the western shore of the Magdalen Shallows (see Fig. 1). All the data in Fig. 11 were smoothed by low-pass filtering with an 18 h cutoff period and are plotted at 6 h intervals. The filter was applied after the mean-square values had been calculated, but before the square roots were taken.

The data of Fig. 11 are replotted in Fig. 12 in the form of rms residual current versus mean-square wind speed. Despite considerable scatter, the data show a convincing linear trend. The solid line represents a least-squares fit, where the correlation coefficient r, resulting from the linear regression, was $r = 0.71$. The least-squares fit is represented by

$$\sqrt{(u^2 + v^2)}_{\text{av}} = 0.074\ W^2 + 12, \qquad (1)$$

where $\sqrt{(u^2 + v^2)}_{\text{av}}$ is the rms current (cm s^{-1}) and W^2 is the mean-square wind speed [(m s^{-1})^2]. The residual current (12 cm s^{-1}) which remains when the wind speed is zero may also be partly due to the wind since the wind-induced currents persist for a day or so after the wind has stopped blowing. This point is discussed further in the theory section.

4. Theory

a. Simplified model for inertial currents

We use a vertically integrated slab model with wind stress forcing at the surface and a linear drag law at the bottom, similar to that used by Pollard and Millard (1970). The equations of motion for the slab are (neglecting pressure gradients and nonlinear terms)

$$\frac{\partial u}{\partial t} - fv + \frac{R}{\rho H} u = \frac{\tau_{sx}}{\rho H}, \qquad (2)$$

$$\frac{\partial v}{\partial t} + fu + \frac{R}{\rho H} v = \frac{\tau_{sy}}{\rho H}, \qquad (3)$$

where u and v are the vertically averaged horizontal velocity components, f is the Coriolis parameter, H the thickness of the slab, ρ the average water density, τ_s the wind stress at the surface and R the bottom drag coefficient. Combining Eq. (2)

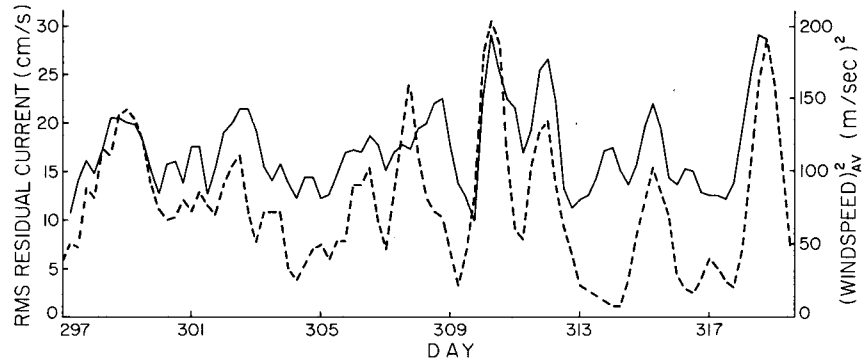

FIG. 11. Root-mean-square residual current (solid line) and mean-square wind speed (dashed line) plotted versus time.

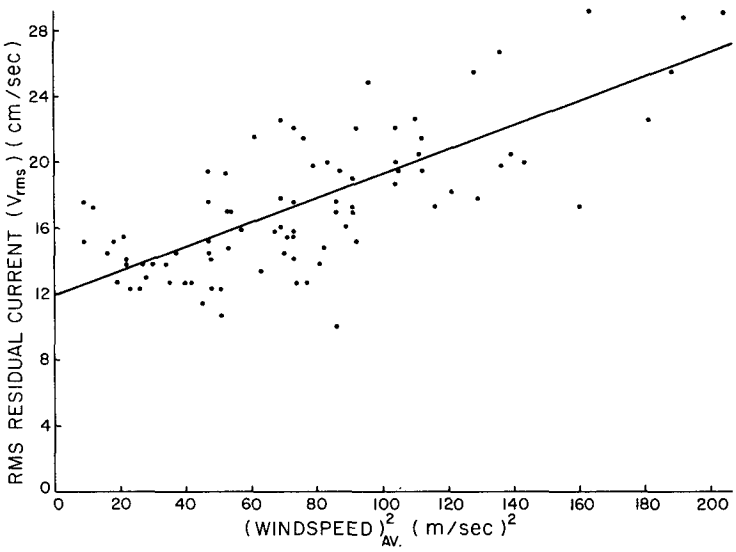

FIG. 12. Root-mean-square residual current plotted versus mean-square wind speed.

and (3) and assuming for the moment that $\tau_{sy} = 0$ then gives

$$\frac{\partial^2 v}{\partial t^2} + 2K\frac{\partial v}{\partial t} + (f^2 + K^2)v = -\frac{\tau_{sx} f}{\rho H}, \quad (4)$$

where $K = R/\rho H$. Eq. (4) is analogous to the equation of a damped harmonic oscillator with forcing, in this case by the wind stress. The natural frequency of oscillation is f, regardless of the value of the damping coefficient K. In this respect, the system behaves differently from the usual mechanical harmonic oscillator, for which the natural frequency decreases with increased damping.

Recalling from Fig. 9 that the wind stress is characterised by a series of random pulses separated by periods of relative calm, it is reasonable to look at the *transient* response of the system to an individual wind stress pulse. We simulate a given wind stress pulse by the form

$$\left.\begin{aligned} \tau_{sx} &= \tau_{0x} \sin\nu t, \quad 0 \leqslant \nu t \leqslant \pi \\ \tau_{sx} &= 0, \qquad\qquad \text{otherwise} \end{aligned}\right\}, \quad (5)$$

where τ_{0x} is the amplitude of the wind stress pulse and it is assumed that the wind stress does not change direction for the entire duration of the pulse. Using Eq. (5) in Eq. (4) and assuming that $v = \dot{v} = 0$ at $t = 0$ then gives the solution (valid for $0 \leqslant \nu t \leqslant \pi$)

$$v = \frac{\tau_{0x}}{\rho H[(f^2 + K^2 - \nu^2)^2 + (2K\nu)^2]^{1/2}} \times \left[f\cos(\nu t + \phi) - f\frac{\cos\phi}{\cos\phi_d} \times e^{-Kt}\cos(ft + \phi_d)\right], \quad (6)$$

where

$$\phi = \tan^{-1}\left(\frac{f^2 + K^2 - \nu^2}{2K\nu}\right), \quad (7)$$

$$\phi_d = \tan^{-1}\left(\frac{\nu}{f}\tan\phi - \frac{K}{f}\right). \quad (8)$$

The first term inside the square brackets of Eq. (6) represents the steady-state portion of the solution, while the second term is the transient ringing at the natural frequency f. Note that the latter term decays with a characteristic time $t = K^{-1}$.

The u component of the slab velocity can now be obtained from Eq. (3) using Eq. (6) and the fact that $\tau_{sy} = 0$. Combining the resulting expression for u with v from Eq. (6) then gives the current amplitude (valid for $0 \leqslant \nu t \leqslant \pi$)

$$(u^2 + v^2)^{1/2}/\tau_0 = \frac{f}{\rho H[(f^2 + k^2 - \nu^2)^2 + (2K\nu)^2]^{1/2}} \times \left\{\left(\frac{\cos\phi}{\cos\phi_d}e^{-Kt}\right)^2 + [(\nu/f)\sin(\nu t + \phi) - (K/f)\cos(\nu t + \phi)]^2 - 2\left[\frac{\cos\phi}{\cos\phi_d}e^{-Kt}\right] \times [\cos(ft + \phi_d)\cos(\nu t + \phi) + \sin(ft + \phi_d) \times [(\nu/f)\sin(\nu t + \phi) - (K/f)\cos(\nu t + \phi)]] + \cos^2(\nu t + \phi)\right\}^{1/2}. \quad (9)$$

In Eq. (9), the restriction that $\tau_{sy} = 0$ has been relaxed and τ_{0x} has been replaced by τ_0, the ampli-

tude of the wind stress pulse regardless of direction. Since there is no preferred direction in the horizontal plane, the amplitude of the current resulting from a given wind stress pulse should not depend on the direction of the wind stress pulse. Examination of the original wind records showed that the assumption of a constant wind direction was a good approximation for most, but not all, of the wind stress pulses in Fig. 9.

When the wind stress pulse cuts off at $\nu t = \pi$, the current amplitude begins to decay with the characteristic time constant K^{-1}, i.e.,

$$(u^2 + v^2)^{1/2}/\tau_0 = A \exp\{-K[t - (\pi/\nu)]\} \quad (10)$$

valid for $t > \pi/\nu$ and where the constant A is equal to the value of $[(u^2 + v^2)^{1/2}]/\tau_0$ in Eq. (9) at $\nu t = \pi$. Therefore, Eqs. (9) and (10) taken together give an expression for the current amplitude response to a given wind stress pulse. It represents the *entire* response to the wind stress pulse, including both the steady state and transient terms. Note that there is an important distinction here between inertial current, which refers to the entire response, and inertial oscillation, which refers only to the transient at the inertial frequency. In the present system a typical wind stress pulse is such as to produce steady-state and transient terms of about the same magnitude. When the wind stress pulse cuts off, the subsequent motion is that of a decaying inertial oscillation, Eq. (10). Before showing the form of this response the unknown parameters in these equations must be determined.

b. Determination of the bottom drag coefficient

The parameters H and K are essentially the only unknowns in Eq. (9). We set H equal to 40 m which was the typical pycnocline depth observed in the Magdalen Shallows during the period of the current meter measurements (Taylor, 1975). Note that this is not much different than the typical total depth of ~60 m. The damping constant K can be determined from the current meter records, as follows. According to Eq. (6) the v velocity component at the pure inertial frequency f decays exponentially with an e-folding time equal to K^{-1}. The same is true for the u velocity component. The square of the current amplitude at the inertial frequency should therefore decay with an e-folding time equal to $(2K)^{-1}$. Fig. 6 shows the time dependence of u and v velocity components at frequency f and Fig. 7 shows the square of the current amplitude at frequency f. The decay of the curves in both figures is quite well approximated by an exponential form which allows one to determine a value for K.

Proceeding in this way, nine independent values of K were determined using the bandpassed data from several current meter stations. The mean value of K was 6.8×10^{-6} s^{-1}, with rms derivation of 1.6×10^{-6} s^{-1}. This value for K gives an e-folding time of 41 h, or 2.5 inertial periods. These values represent a much faster decay of the inertial current amplitude than that found in the deep ocean by Pollard and Millard (1970). A faster decay is expected for the shallower water in the Magdalen Shallows, due to bottom drag.

Using the above value of K it is possible to obtain a rough estimate of the bottom drag coefficient. Recall that $R = K\rho H$, and let R be of the form $R = C_B \rho V_0$, where C_B is the dimensionless bottom drag coefficient and V_0 is a typical current velocity magnitude. Then $C_B = KH/V_0$ and using the above values of K and H and taking $V_0 \approx 10$ cm s^{-1} gives $C_B \simeq 2.7 \times 10^{-3}$, which agrees quite well with currently accepted values (e.g., Tee, 1976) of the bottom drag coefficient.

c. Current response to a wind stress pulse

Fig. 13 shows the predicted current amplitude response from Eqs. (9) and (10) plotted versus νt up to $\nu t \approx 2\pi$, for three different values of ν, using the values of H and K given above. The dashed curve in Fig. 13 shows the sinusoidal wind stress pulse which cuts off at $\nu t = \pi$. The response to the wind stress pulse is considerably different for the three values of ν shown, i.e., $\nu = f/2, f/3$ and $f/5$. The largest response occurs for $\nu = f/2$ and the strongest inertial oscillation remains, after the wind stops, for this case also. The response for $\nu = f/3$ follows the wind stress pulse most closely. A double peak occurs in the response for $\nu = f/5$, which is due to the terms containing the inertial frequency in Eq. (9).

Fig. 14 shows the current amplitude responses plotted versus actual time in hours. The corresponding wind stress pulses are not shown but the times at which the wind cuts off are indicated by the arrows, for each value of ν. For example, the wind stress pulse corresponding to $\nu = f/2$ lasts for a period of 16 h. The response for $\nu = f$ was also calculated and was found to be considerably less than that for $\nu = f/2$, which suggests that the response is maximum at $\nu \sim f/2$. The latter result appears to conflict with a statement by Pollard and Millard (1970) who conclude that "a wind vector acting in one direction for one inertial period would generate no inertial current, since it would remove as much momentum in the second half period as it added in the first". Assuming that the magnitude of the wind vector was also constant, this would be true in the absence of friction. However, neither of these conditions is appropriate for the Magdalen Shallows and the result is not true in this case.

Generally speaking, it can be said that the results in Figs. 13 and 14 show that the response of the

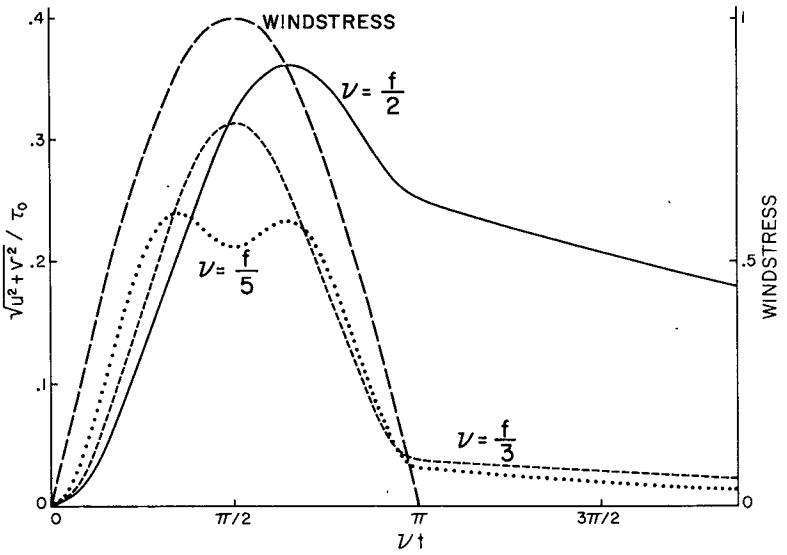

FIG. 13. Predicted current amplitude response to a sinusoidal wind stress pulse for the time interval $0 \leq \nu t \leq 2\pi$. The wind stress cuts off at $\nu t = \pi$. The responses for three different values of ν are shown.

simplified model to a wind stress pulse is also pulselike with a relatively short phase lag. The behavior is not unlike that shown in Fig. 11 for the real system. The strength of the pure inertial oscillation remaining after the pulse is a rather sensitive function of the time duration of the pulse. This could explain why the pure inertial oscillation was strong in some cases and weak in others, i.e., poorly correlated with the wind. On the other hand, the rms amplitude of the response is considerably less erratic, a fact which no doubt helps to explain the better correlation with the wind in this case.

d. Determination of the wind drag coefficient

By comparing the theoretical relationship between wind stress and current with Eq. (1) it is possible to extract a value for the wind drag coefficient at the air-sea interface. The procedure was as follows. The theoretical results in Fig. 14 were

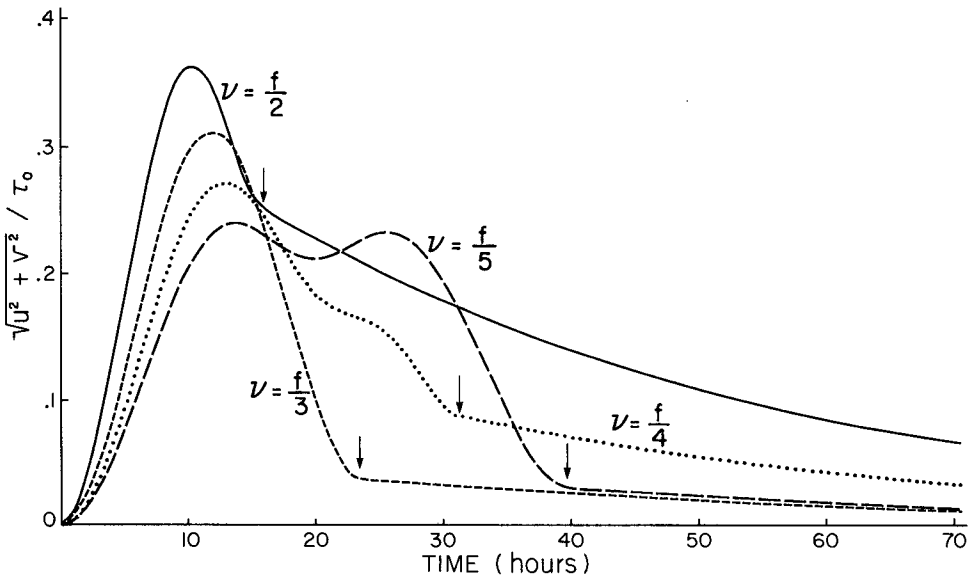

FIG. 14. Predicted current amplitude response plotted versus time in hours. The responses for four different values of ν are shown.

used to carry out a linear regression (from $t = 0$ to $t = 60$ h) between the sinusoidal wind stress pulse and the resulting current amplitude, assuming only one wind stress pulse in a 60 h interval. The analysis was done for each value of ν and the resulting linear relationships were different for each case. From Fig. 11 it can be seen that the majority of wind stress pulses last for periods of somewhat less than one day to about two days. Corresponding to this a linear regression was therefore done only on the combined data for $\nu = f/2$, $f/3$, $f/4$ and $f/5$, giving equal weight to each value of ν. This gave the following linear fit between wind stress and current (correlation coefficient $r = 0.76$)

$$(u^2 + v^2)^{1/2} = 0.24\tau + 0.033\tau_0, \qquad (11)$$

where τ is the instantaneous value of the wind stress and τ_0 is the magnitude of the wind stress at the peak of the pulse. τ has the form shown in Fig. 13, i.e., a pulse followed by a period of zero wind stress. Comparing Eq. (11) with Eq. (1) and assuming the usual relationship ($\tau = C_D \rho_a W^2$) between wind stress and wind speed then gives $0.24\ C_D \rho_a W^2 = 7.4 \times 10^{-4}\ W^2$ and therefore $C_D \approx 2.5 \times 10^{-3}$, where C_D is the wind drag coefficient and ρ_a is the density of air. This value for C_D agrees reasonably well with the values obtained by more direct measurements ($C_D = 1.5 \times 10^{-3}$) (e.g., Smith and Banke, 1975). We do not pretend to have obtained a useable value of C_D but merely wish to show the self-consistency of the model used.

The constant term in Eq. (11) can also be estimated by using a typical value for τ_0, the wind stress maximum. From Fig. 11, the latter is readily estimated to be about 6 dyn cm^{-2}, which gives a value of 2 cm s^{-1} for the constant term in Eq. (11). Recalling that the corresponding constant term in Eq. (1) was 12 cm s^{-1} then leaves (in a crude sense) a current speed of about 10 cm s^{-1} which is not accounted for by the simple model. The latter may be due to geostrophic currents associated with the remnants of the Gaspé current, as it disperses over the Magdalen Shallows.

5. Concluding remarks

The analysis showed that inertial oscillations were a characteristic feature of the residual currents in the Magdalen Shallows during the measurement period. This suggests that the system was not in a steady state but rather passed from one transient state of excitation to the next. The random pulse-like nature of the wind stress is consistent with the above behavior and makes the wind a prime candidate for the driving force. The transient response, to the wind, of the simple slab model studied gave a surprisingly good representation of the observed behavior.

The assumption of zero initial slab velocity prior to a wind stress pulse [i.e., $v = \dot{v} = 0$ in the derivation of Eq. (6)] is probably one of the more serious approximations made in the model. Even if the wind induced motion decays between pulses there are still the convection currents and also the tidal currents. A more rigorous approach would be to take the initial velocities into account but, due to the increased complexities which arise, this was not attempted.

The behavior of the system at other seasons of the year is interesting to consider. For example, Eq. (9) suggests that the amplitude of the response may be larger when the pycnocline depth H is smaller, such as during the summer months. On the other hand, the damping coefficient K may also be different, making the net result uncertain.

Acknowledgments. Thanks are extended to numerous colleagues at the Bedford Institute of Oceanography for helpful discussions. I particularly wish to thank Dr. Allyn Clarke for assistance in the operation of his computer programs used for current meter data analysis. The Coastal Oceanography Division provided financial support and allowed free access to the current meter records.

REFERENCES

Dobson, F., R. F. Brown and D. R. Chang, 1974: A set of programs for analysis of time series data including fast Fourier transform spectral analysis. Rep. BI-C-74-2, Bedford Institute of Oceanography, Dartmouth, N.S., Canada, 157 pp.

El-Sahb, M. I., 1975: Transport and currents in the Gulf of St. Lawrence. Rep. BI-R-75-9, Bedford Institute of Oceanography, Dartmouth, N.S., Canada, 180 pp.

Farquharson, W. I., 1966: St. Lawrence estuary current surveys. Rep. BIO 66-6, Bedford Institute of Oceanography, Dartmouth, N.S., Canada, 84 pp.

Pollard, R. T., and R. C. Millard, Jr., 1970: Comparison between observed and simulated wind-generated inertial oscillations. *Deep-Sea Res.*, **17**, 813–821.

Kundu, Pijush K., 1976: An analysis of inertial oscillations observed near Oregon Coast. *J. Phys. Oceanogr.*, **6**, 879–893.

Smith, S. D., and E. G. Banke, 1975: Variation of the sea surface drag coefficient with wind speed. *Quart. J. Roy. Meteor. Soc.*, **101**, 665–673.

Taylor, George B., 1975: Oceanographic observations in the Magdalen Shallows and Gulf of St. Lawrence from 25 Oct. to 16 Nov. 1970. Rep. BI-D-75-7, Bedford Institute of Oceanography, Dartmouth, N.S., Canada, 86 pp.

Tee, Kim-Tai, 1976: Tide induced residual current: A 2-D nonlinear numerical tidal model. *J. Mar. Res.*, **34**, 603–628.